Research on NCF-PCF-NCF Structure Interference Characteristic for Temperature and Relative Humidity Measurement

Jietong Zhang, Zhengrong Tong, Weihua Zhang, Yeming Zhao, and Yixi Liu

***Abstract*—A novel structure of photonic crystal fiber (PCF) Mach-Zehnder interferometer (MZI) for temperature and relative humidity measurement is proposed. The novel structure is composed of two sections of no core fiber (NCF) with a piece of PCF. The sensitivity of the proposed sensor is enhanced by adopting NCF coupling method. The results show that the sensitivities of temperature are 0.059 nm/°C, 0.074 nm/°C and 0.130 nm/°C in the range of 25 °C to 70 °C, and the sensitivities of relative humidity are 0.020 nm/% RH, 0.027 nm/% RH and 0.036 nm/% RH in the range of 30% RH to 70% RH. The sensor has the advantages of high stability, good linearity fit and simple structure, which indicates that the sensor has the potential of making an important contribution to the field of biology, chemistry, and medical.**

***Index Terms*—Photonic crystal fiber, temperature, relative humidity, Mach-Zehnder interferometer, no core fiber coupling.**

I. Introduction

In THE recent years, fiber optic interferometers have been widely used due to their unique advantages of good stability, high sensitivity, anti-electromagnetic interference, and corrosion resistance [1]–[5]. The size of optical fiber is small, and it can be fused into a variety of forms. Based on this property of optical fiber, researchers have designed and fabricated all kinds of Mach-Zehnder interferometers (MZIs). The MZIs are applied to the measurement of physical and chemical parameters such as temperature [6], relative humidity [7], strain [8], refractive index (RI) [9], liquid level [10], and glucose concentration [11], etc.

The principle of MZI is that some physical properties of the cladding modes in an optical fiber are affected by the external environment, and interference occurs due to the coupling of core modes and claddings. In this process, the different coupling methods will also make the fiber optic sensors have different properties. The coupling methods of fiber optic sensors are spherical structure [12], tapered structure [13], peanut-sharp structure [14], off-axis twisted deformation structure [15] and different fiber coupling [16]. In 2018, Tong *et al.* [17] designed a novel in-line mode MZI based on coated graphene quantum dots (GQDs) and polyvinyl alcohol (PVA) films for relative humidity sensing. The MZI was formed by splicing a segment of PCF between two segments of single-mode fiber (SMF) with two spherical structures. The relative humidity sensitivities of proposed sensor coated with different thickness of GQDs-PVA film (2.48 m, 3.72 m, 4.45 m, 5.96 m, 7.42 m, 8.17 m) were −0.0901 nm/%RH, −0.0797 nm/%RH, −0.0337 nm/%RH, 0.0586 nm/%RH, 0.0539 nm/%RH, 0.0313 nm/%RH, respectively. In 2019, Yu *et al.* [18] proposed an in-line MZI for RI and temperature sensing. The structure was a cascade of two peanut-shape structures at the ends of a section of single-mode fiber (SMF). The operational performance of RI and temperature measurements with two different intermediate sensing lengths (30 mm and 100 mm) was researched. The sensor with a long sensing length of 100 mm was capable of measuring temperature and RI simultaneously and eliminating the cross-sensitivity of temperature and RI. The highest RI and temperature sensitivity were -67.953 nm/RIU and 0.073 nm/°C respectively. In the same year, Wang *et al.* [19] designed and implemented a novel in-line MZI system based on a single-mode-thin-core-single-mode fiber structure for temperature sensing, which is manufactured by tapering an optical fiber. The experimental results showed that a temperature sensitivity is 65 pm/°C in the range of 25 °C to 80°C the linear correlation coefficient is 0.996. The essential difference between this MZI and the previously reported MZI was that this sensor was based on the splicing area of the SMF and the thin core fiber (TCF) to pull the taper to excite the evanescent wave for better interference. In 2020, Liu *et al.* [20] proposed a TCF and ultrathin fiber (UTF) based MZI for temperature and RI measurement, where TCF and UTF were used to be sensing and coupling, respectively. The researchers conducted experiments using 14 mm TF and 1 mm UTF. The maximum sensing sensitivities were −169.0879 nm/RIU and 0.0464 nm/°C, respectively. The length of the UTF effectively affected the mode coupling coefficient and interference spectrum, and the sensitivity of the sensor was improved.

In this paper, a NCF-PCF-NCF(NPN) structure MZI for temperature and relative humidity measurement is demonstrated. This novel structure sensor is achieved by splicing a section of PCF with two sections of NCF. The sensitization effect of this

Manuscript received June 4, 2021; revised August 12, 2021; accepted August 12, 2021. Date of publication August 23, 2021; date of current version September 9, 2021. This work was supported in part by the Natural Science Foundation of Tianjin City under Grant JCYBJC86300, and in part by Tianjin Research Innovation Project for Postgraduate Students under Grant 2020YJSS016. *(Corresponding author: Zhengrong Tong.)*

The authors are with the Engineering Research Center of Optoelectronic Devices and Communication Technology, Ministry of Education, Tianjin Key Laboratory of Film Electronic and Communication Devices, School of Integrated Circuit Science and Engineering, Tianjin University of Technology, Tianjin 300384, China (e-mail: zhangjietong315@163.com; tjtongzhengrong@163.com; nmgzwh@163.com; tjzhaoyeming@163.com; 2243751633@qq.com).

Digital Object Identifier 10.1109/JPHOT.2021.3105395

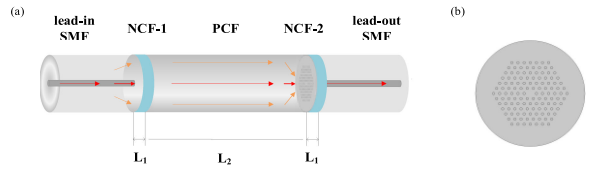

Fig. 1. (a) Schematic diagram of the sensor based on NPN structure (b) Cross-section of LMA-10.

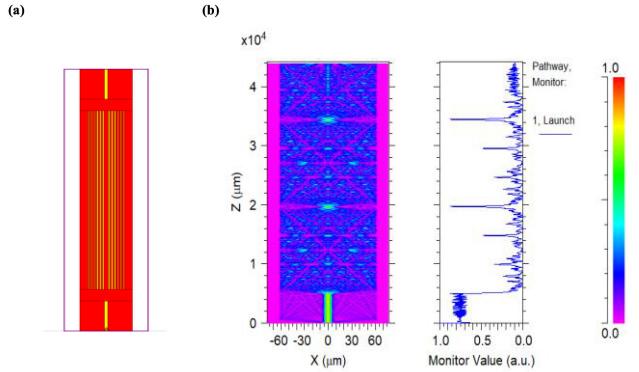

Fig. 2. (a) The simulation model of NCF-PCF-NCF structure in Rsoft (b) Simulation diagram of light energy x-z plane of the proposed MZI.

coupling method has been experimentally proved to be significant. By comparing the temperature and relative humidity experiments results with the ones of the MMF-PCF-MMF(MPM) structure fiber sensor, the dips of the sensor of NPN structure have higher sensitivities to the parameters, which indicates that the proposed sensor in this paper is more practical for temperature and humidity measurement.

II. Sensor Construction and Theory

The schematic diagram of the sensor based on NPN structure is shown in Fig. 1(a). The length L_2 of the PCF is 3 cm and the lengths L_1 of both NCF-1 and NCF-2 for coupling are 2 mm. The MZI consists of a lead-in SMF, a NPN structure and a lead-out SMF. The SMF model is SMF-28 with core diameter and cladding diameter of 8.2 μm and 125 μm respectively. The cross-section view of the PCF (LMA-10 of NKT) is shown in Fig. 1(b). The PCF consists of six layers of air holes and the diameters of core and cladding are 10.1 μm and 125 μm respectively. The cladding diameter of NCF (CL1010-A, YOFC) is 125 μm. The MZI is fabricated by the following steps:

The lead-in SMF with a cleaved end and NCF-1 are placed at each end of the fusion splicer and fixed. The fusion splice is performed by selecting the cc-cc mode fusion splice program in the fusion splicer (Fitel, S178C, by Japan). During the fusion process, the discharge intensity and discharge duration are optimized to be 30 and 300 ms, for the splicing PCF and NCF-1 respectively. And then the NCF-2 is spliced with PCF by using the same splicing program. The diagram of NPN sensor structure is shown in Fig. 1 (a).

Fig. 2 (b) shows the modal characteristics of the sensor transmission studied by the BeamProP module of Rsoft. When the light is transmitted from the lead-in SMF to NCF-1, the light is leaked out from the core into the cladding due to the mismatch of the cores of the fibers, which in turn creates a cladding pattern. The transmitted energy is redistributed when the light reaches the fusion point between NCF-1 and PCF, and then it is transmitted in the sensing area. When the core mode and the cladding modes are transmitted to NCF-2, the interference occurs due to the certain phase conditions of light is satisfied and part of the cladding modes are re-coupled into the SMF at the output, then interference is formed.

The interference spectrum is formed by the interference between the core mode and the cladding modes of different orders, so the total light intensity when the sensor interferes can be equivalently expressed as [21]:

$$I = I_{core} + \sum_i I_{clad}^i + 2\sum_i \sqrt{I_{core} I_{clad}^i} \cos \Delta\varphi_{core-clad} \tag{1}$$

where I is the total light intensity, I_{core} is the intensity of the core mode, and I_{clad}^i is the intensity of cladding modes. At this point the phase difference $\Delta\varphi_{core-clad}$ can be expressed as:

$$\Delta\varphi_{core-clad} = \frac{2\pi\Delta n_{eff}}{\lambda} L \tag{2}$$

where L is the length of the sensing fiber and λ represents the wavelength of the incident light. Δn_{eff} is the difference of the effective refractive index of the core mode (n_{eff}^{core}) and the cladding modes (n_{eff}^{clad}). It can be expressed as:

$$\Delta n_{eff} = n_{eff}^{core} - n_{eff}^{clad} \tag{3}$$

In summary, when $\Delta\varphi_{core-clad} = (2\mathrm{m}+1)\pi$ (where m is an integer), the phase difference in Eq. (2) reached the minimum value. The wavelength of the interference dip can be expressed as:

$$\lambda_{dip} = \frac{2\Delta n_{eff} L}{2m+1} \tag{4}$$

Therefore, the free spectrum range (FSR) of the interference spectra can be approximated as [22]:

$$FSR \approx \frac{\lambda^2}{\Delta n_{eff} L} \tag{5}$$

The internal structure parameters of the fiber are changed because of the change of the external environment temperature, and the wavelength change of interference dip affected by temperature can be expressed as:

$$\Delta\lambda_{dip} = \lambda_{dip}\left(\alpha + \frac{\xi_{core} n_{core} - \xi_{clad} n_{clad}}{\Delta n_{eff}}\right)\Delta T \tag{6}$$

where ξ_{core} and ξ_{clad} are the effective thermo-optic coefficients of the core and the cladding modes, respectively. α is the coefficient of thermal expansion. The temperature sensitivity of the proposed sensor can be calculated according to Eq. (6) as:

$$K_T = \frac{\Delta\lambda_{dip}}{\Delta T} = \lambda_{dip}\left(\alpha + \frac{\xi_{core} n_{core} - \xi_{clad} n_{clad}}{\Delta n_{eff}}\right) \tag{7}$$

Relative humidity is a fundamental physical parameter related to RI. The change of water vapor concentration in the air causes a change in the RI around the sensor. The variation of the dominant cladding pattern with respect to the variation of the

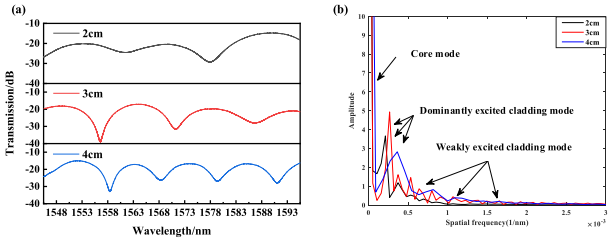

Fig. 3. (a) Transmission spectra of the proposed MZI with different sensing length (b) spatial frequency spectra of different sensing length.

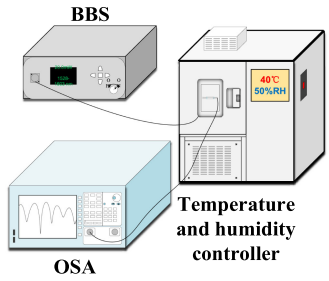

Fig. 4. The schematic diagram of the temperature and relative humidity experiment.

external refractive index is $\Delta n_{clad} = \frac{\partial n_{clad}}{\partial RI}\Delta RI$. Therefore, the RI sensitivity of the proposed sensor can be calculated as:

$$K_{RI} = \frac{\Delta\lambda_{eff}}{\Delta RI} = \frac{2L}{2m+1} \cdot \frac{\partial n_{clad}}{\partial RI} \tag{8}$$

Water vapor forms a wet film on the sensor surface and the force exerted on the structure varies with the relative humidity. The sensitivity of relative humidity can be approximated as:

$$K_{RH} = \frac{2L}{2m+1} \cdot \frac{\partial n_{clad}}{\partial RH} \tag{9}$$

III. Experimental Procedure and Analysis of Results

A. Different Length Comparison Experiment of NPN Structure

Before carrying out the temperature and relative humidity measurements. Three PCF sensors with lengths of 2 cm, 3 cm and 4 cm are fabricated respectively, and necessary comparative PCF lengths analysis is performed. The comparative transmission spectra of the three lengths are shown in Fig. 3 (a). FSR decreases with the increasing of L, which is consistent with the analysis of Eq. (5). When the PCF is 3 cm, there are three obvious interference dips near 1553 nm,1569 nm and 1583nm in the interference spectrum. The spectrum of the sensor has the highest extinction ratio (ER) of ∼22.5 dB, and the dynamic measurement range is large, which can be used to analyze the temperature and relative humidity characteristics of the sensor. The transmission spectrum corresponding to the fast Fourier transform (FFT) is shown in Fig. 3 (b) [23]. Compared to the other two sensors, the one with the length of sensing area of 3cm has a higher dominant peak. When PCF is 3 cm, the peak difference between the core mode and the cladding modes is large, which indicates that the interference mode of the sensor is very stable during the occurrence of interference. Therefore, a 3cm PCF is used as the sensing area of the MZI in this paper.

B. Temperature and Relative Humidity Experiment of NPN Structure

The schematic diagram of the temperature and relative humidity experiment is shown in Fig. 4. The broadband source (BBS) provides the optical energy for the experiment with an output wavelength range of 1528-1603 nm. The interference spectrum can be observed by the optical spectrum analyzer (OSA, AQ6370D by Yokogawa). The resolution of OSA is 0.02 nm. The environmental parameters are controlled by adjusting the temperature and humidity controller.

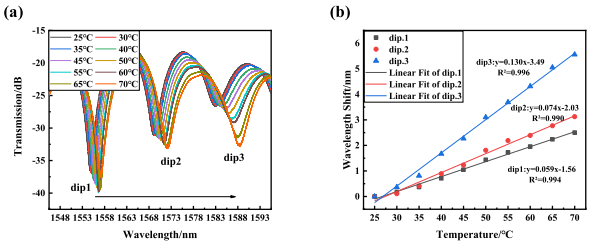

Fig. 5. (a) Comparison of the transmission spectra of sensor based on NPN structure at 25 °C to 70 °C (b) wavelength shift and linear fitting of dip1, dip2, and dip3.

The temperature characteristics of the proposed sensor with NPN structure are investigated. The sensor is placed horizontally inside temperature and humidity controller that maintains a humidity level of 40%RH. The temperature is increased in the steps of 5 °C from 25 °C to 70 °C. Ten groups of temperature experiment data are recorded. The interference spectra in OSA are recorded once when it is stable. The variations of the interference spectra in the temperature experiments are shown in Fig. 5(a). It's clear to see that as the temperature increases, the dip1∼dip3 are redshift. Fig. 5(b) shows the temperature linear fitting diagram of dip1∼dip3. The temperature sensitivities of the selected dips are 0.059 nm/°C, 0.074 nm/°C and 0.130 nm/°C and the linear fits of the dip1∼dip3 are 0.994, 0.990 and 0.996 respectively. The experimental results show that the proposed sensor has the advantages of high sensitivity, and good stability.

The relative humidity characteristics of the proposed sensor with NPN structure are explored. The sensor is placed horizontally inside temperature and humidity controller that maintains a temperature level of 25 °C. The relative humidity starts at 30%RH and increases to 70%RH at intervals of 5%RH. The transmission spectra are saved by OSA when the temperature and relative humidity are stable. Nine groups of relative humidity experiment data are recorded. As shown in Fig. 6 (a), the wavelengths of dip1∼dip3 are shown redshift. Fig. 6 (b) is the relative humidity fitting diagram of the dip1∼dip3 of the sensor with NPN structure. The relative humidity sensitivities are 0.020 nm/%RH, 0.027 nm/%RH and 0.036 nm/%RH with fitting linearity of 0.998, 0.990 and 0.991, respectively.

Stability is an important parameter to determine the performance of a sensor. To study the stability of the sensor, another temperature experiment is carried out. The sensor is placed in the ambient temperature of 25 °C and 70 °C. The interference

TABLE 1
THE FLUCTUATION RANGE IN TEMPERATURE STABILITY EXPERIMENT

	Fluctuation range of the central wavelength at 25°C(nm)		difference value(nm)	Fluctuation range of the central wavelength at 70°C(nm)		difference value(nm)	Temperature sensitivity(nm/℃)
dip1	1554.736	1554.792	0.056	1557.152	1557.204	0.052	0.059
dip2	1569.012	1569.076	0.064	1572.084	1572.148	0.064	0.074
dip3	1583.036	1583.084	0.048	1588.388	1588.432	0.044	0.130

THE FLUCTUATION RANGE IN RELATIVE HUMIDITY STABILITY EXPERIMENT

	Fluctuation range of the central wavelength at 30%RH (nm)		difference value(nm)	Fluctuation range of the central wavelength at 70%RH (nm)		difference value(nm)	Relative humidity sensitivity(nm/%RH)
dip1	1556.636	1556.652	0.016	1557.374	1557.384	0.01	0.020
dip2	1570.868	1570.892	0.024	1571.98	1571.996	0.016	0.027
dip3	1586.364	1586.382	0.018	1587.748	1587.756	0.008	0.036

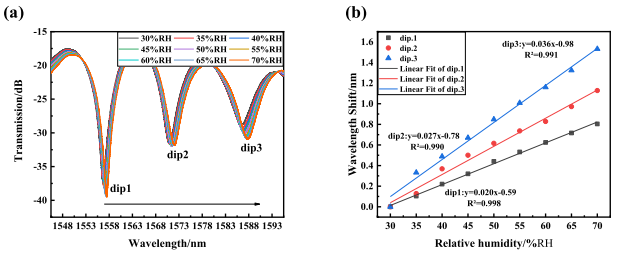

Fig. 6. (a) Comparison of the transmission spectra of sensor based on NCF-PCF-NCF structure at 30%RH to 70%RH (b) wavelength shift and linear fitting of dip1, dip2, and dip3.

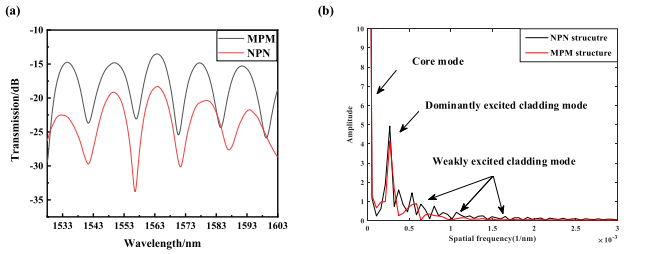

Fig. 8. (a) Transmission spectra of NPN and MPM (b) spatial frequency spectra of NPN and MPM.

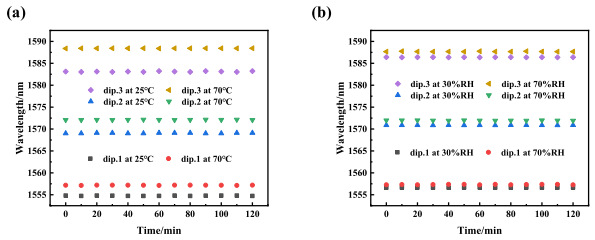

Fig. 7. (a) Schematic diagram of temperature stability experiment (b) Schematic diagram of relative humidity stability experiment.

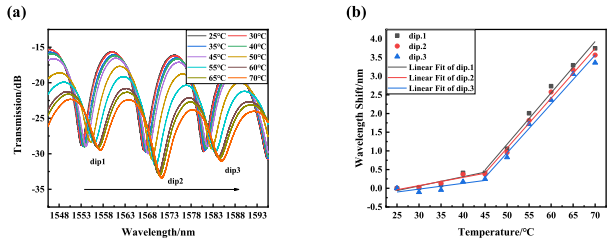

Fig. 9 (a) Comparison of the transmission spectra of sensor based on MPM structure at 25°C to 70°C (b) wavelength shift and linear fitting of three dips.

spectra are recorded every 10 minutes for two hours of observation. The measurement results of the stability experiment are shown in Fig. 7. In the humidity stability experiment, the sensor is placed following the same way in former experiment, and the data are recorded. It can be seen from Fig. 7 (a) and Fig. 7 (b) that the same resonant interference dips have a small fluctuation within two hours of the measurement, which indicates that the sensor has a good measurement stability.

As shown in Table 1, in the temperature and relative humidity sensing experiments, the maximum fluctuation values don't exceed the sensitivity corresponding to their interference dips. The fluctuation range can be neglected in the temperature and relative humidity experiments.

C. Temperature and Relative Humidity Experiment of MPM Structure

There are different transmission modes in different fibers, so different higher order modes in the sensing fiber are also stimulated when fibers are used for coupling. In order to compare the effects on the sensor when different fibers are used for coupling, the same length of MMFs are used instead of the NCF in the proposed structure of the sensor. The diameter of the core and cladding of multimode fiber are 105 μm and 125 μm, respectively. Fig. 8 (a) shows a comparison between the interference spectra of the NPN sensor and MPM sensor. Both NPN sensor and MPM sensor have three interference dips in the observed range and they have similar FSR. But NPN sensor has a higher extinction ratio. As shown in Fig. 8 (b), according to FFT result, it is obvious that the dominant interference peak of NPN sensor is higher than that of MPM sensor. There are more modes involved in the interference in NPN sensor and the peak difference between the peaks formed by the core mode and the cladding modes of each order is large, which indicates that the sensor is very stable during the occurrence of the interference.

Next, the same temperature and relative humidity experiments using MPM sensor are carried for which kind of fiber is more applicable for coupling in sensor. Fig. 9 (a) shows the transmission spectra change of MPM sensor. It can be seen that

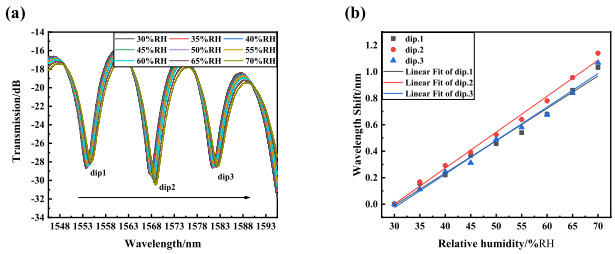

Fig. 10 (a) Comparison of the transmission spectra of sensor based on MPM structure at 30%RH to 70%RH (b) wavelength shift and linear fitting of three dips.

the wavelength of dip1∼dip3 experience a red shift when the temperature increases in the range of 25 °C to 70 °C. The linear fitting of the selected dip wavelength changes is illustrated in Fig. 9(b). The temperature sensitivities of the selected dips are 0.138 nm/°C, 0.133 nm/°C and 0.131 nm/°C in the range of 45 °C to 70 °C respectively. The linear fits of the three dips' wavelength changes are 0.984, 0.986 and 0.983 respectively. As shown in Fig. 10 (a), it is can be seen that the three dips of interference spectra experience a red shift. The relative humidity sensitivities of the three dips are 0.024 nm/%RH, 0.027 nm/%RH and 0.025 nm/%RH respectively. The linear fits of the three dips' wavelength changes are 0.984, 0.992 and 0.984 respectively.

Comparing the experimental results of NPN sensor and MPM sensor, it can be seen that the interference dips of MPM sensor exhibit the same sensitive characteristics and the fitted curve is not linear in the temperature range of 25 °C to 70 °C. The sensitivity is high at 45 °C to 70 °C, but the linear fitting and stability are low. In contrast, the sensor of NPN structure has a high sensitivity and the interference dips have a sensitivity difference, which is suitable for multiparametric sensing. In the experiments of temperature and humidity, the sensor shows the advantages of high stability and good fitting, and the overall performance is better than the MPM sensor. In summary for the experiment of NPN sensor, NCF is more suitable for optical fiber coupling than MMF.

IV. Conclusion

In this paper, a PCF MZI based on the coupling of NCF for temperature and relative humidity measurement is designed and manufactured. According to the theoretical analysis and experiments results, a novel structure which is a new approach using NCF coupling successfully enhances the sensitivity of temperature. In the meanwhile, NCF is proved an excellent coupling structure for application in micro-structured MZI. The temperature experiment results show the sensor has the highest temperature sensitivity of 0.130 nm/°C. In the range of relative humidity 30%RH to 70%RH, the sensor has the highest humidity sensitivity of 0.036 nm/%RH. The sensor has the advantages of high sensitivity, good stability, high linear fitting, easy fabrication and low cost, which indicate that the device has a great potential in temperature and relative humidity sensing fields.

References

[1] A. G. Leal-Junior *et al.*, "Analysis of viscoelastic properties influence on strain and temperature responses of Fabry-Perot cavities based on UV-curable resins," *Opt. Laser Technol.*, vol. 120, 2019, Art. no. 105743.
[2] S. Pevec and D. Donlagic, "Miniature all-silica fiber-optic sensor for simultaneous measurement of relative humidity and temperature," *Opt. Lett.*, vol. 40, no. 23, pp. 5646–5649, 2015.
[3] L. Sun *et al.*, "Investigation of humidity and temperature response of a silica gel coated microfiber coupler," *IEEE Photon. J.*, vol. 8, no. 6, Dec. 2016, Art. no. 6805410.
[4] S. R. Azzuhri *et al.*, "Application of graphene oxide based microfiber-knot resonator for relative humidity sensing," *Results Phys.*, vol. 9, pp. 1572–1577, 2018.
[5] E. Reyes-Vera, M. B. Cordeiro, and P. Torres, "Highly sensitive temperature sensor using a Sagnac loop interferometer based on a side-hole photonic crystal fiber filled with metal," *Appl. Opt.*, vol. 56, no. 2, pp. 156–162, 2017.
[6] J. Li *et al.*, "High sensitivity temperature probe based on elliptical microfiber knot ring," *Results Phys.*, vol. 16, 2020, Art. no. 102953.
[7] M. Y. Mohd Noor *et al.*, "Temperature-insensitive photonic crystal fiber interferometer for relative humidity sensing without hygroscopic coating," *Meas. Sci. Technol.*, vol. 24, no. 10, 2013, Art. no. 105205.
[8] S. M. Nalawade and H. V. Thakur, "Photonic crystal fiber strain-independent temperature sensing based on modal interferometer," *IEEE Photon. Technol. Lett.*, vol. 23, no. 21, pp. 1600–1602, Nov. 2011.
[9] H. Y. Choi *et al.*, "Cross-talk free and ultra-compact fiber optic sensor for simultaneous measurement of temperature and refractive index," *Opt. Exp.*, vol. 18, no. 1, pp. 141–149, 2010.
[10] W. H. Zhang, Z. S. Ying, S. Yuan, and Z. R. Tong, "A fiber laser sensor for liquid level and temperature based on two taper structures and fiber Bragg grating," *Opt. Commun.*, vol. 342, pp. 243–246, 2015.
[11] B. Q. Jiang *et al.*, "Label-free glucose biosensor based on enzymatic graphene oxide-functionalized tilted fiber grating," *Sens. Actuator B-Chem.*, vol. 254, pp. 1033–1039, 2017.
[12] M. Shao, X. G. Qiao, H. W. Fu, N. Zhao, Q. Liu, and H. Gao, "An in-fiber Mach–Zehnder interferometer based on arc-induced tapers for high sensitivity humidity sensing," *IEEE Sensors J.*, vol. 13, no. 5, pp. 2026–2031, May 2013.
[13] Q. Wang *et al.*, "High sensitivity refractive index sensor based on splicing points tapered SMF-PCF-SMF structure Mach-Zehnder mode interferometer," *Sens. Actuator B-Chem.*, vol. 225, no. 3, pp. 213–220, 2016.
[14] D. Wu *et al.*, "All single-mode fiber Mach–Zehnder interferometer based on two peanut-shape structures," *J. Lightw. Technol.*, vol. 30, no. 5, pp. 805–810, 2012.
[15] Y. Liu, H. F. Lin, Y. T. Dai, and A. Zhou, "Humidity sensor based on an in-fiber integrated Mach-Zehnder interferometer," *IEEE Photon. Technol. Lett.*, vol. 31, no. 5, pp. 393–396, Mar. 2019.
[16] Y. Wu *et al.*, "Highly sensitive curvature sensor based on asymmetrical twin core fiber and multimode fiber," *Opt. Laser Technol.*, vol. 92, pp. 74–79, 2017.
[17] R. J. Tong *et al.*, "Relative humidity sensor based on small up-tapered photonic crystal fiber Mach-Zehnder interferometer," *Sens. Actuator A-Phys.*, vol. 280, pp. 24–30, 2018.
[18] F. D. Yu, P. Xue, X. W. Zhao, and J. Zhang, "Investigation of an in-line fiber Mach-Zehnder interferometer based on peanut-shape structure for refractive index sensing," *Opt. Commun.*, vol. 435, pp. 173–177, 2018.
[19] Q. Z. Wang *et al.*, "Optical fiber temperature sensor based on a Mach-Zehnder interferometer with single-mode-thin-core-single-mode fiber structure," *Rev. Sci. Instrum.*, vol. 91, no. 1, 2020, Art. no. 015006.
[20] W. Liu *et al.*, "Refractive index and temperature sensor based on Mach-Zehnder interferometer with thin fibers," *Opt. Fiber Technol.*, vol. 54, 2020, Art. no. 102101.
[21] X. Bai, D. Fan, S. Wang, S. Pu, and X. Zeng, "Strain sensor based on fiber ring cavity laser with photonic crystal fiber in-line Mach–Zehnder interferometer," *IEEE Photon. J*, vol. 6, no. 4, Aug. 2014, Art. no. 6801608.
[22] F. R. Zheng *et al.*, "Temperature and index insensitive strain sensor based on a photonic crystal fiber in line Mach–Zehnder interferometer," *Opt. Commun.*, vol. 297, no. 12, pp. 7–11, 2013.
[23] Y. Sun *et al.*, "Dual-parameters optical fiber sensor with enhanced resolution using twisted MMF based on SMS structure," *IEEE Sensors J.*, vol. 17, no. 10, pp. 3045–3051, May 2017.